Mao et al. *Zool. Res.* 2025, 46(4): 863−876
https://doi.org/10.24272/j.issn.2095-8137.2024.447
https://cstr.cn/32248.14.zr.2024.447

ZR | Zoological Research

Article Open Access

Subcutaneous delivery of icariin via a gelatin methacryloyl (GelMA) hydrogel sustained-release system improves ovarian function in reproductively aged mice

Jia-Lian Mao[1], Xiang-Yi Wu[2], Ling-Xi Li[1], Ning Li[1], Ya-Xuan Wang[3], Zhi-Wei Jiang[1], Chuan-Ming Liu[4,5], Hui-Dan Zhang[4,5], Ji-Dong Zhou[4,5], Yang Zhang[4,5], Li Chen[6], Gui-Jun Yan[4,5], Hai-Xiang Sun[4,5,7,*], Yi-Fan Li[4,5,*], Li-Jun Ding[1,3,4,5,8,9,*]

[1] *Center for Reproductive Medicine and Obstetrics and Gynecology*, *Nanjing Drum Tower Hospital*, *Clinical College of Nanjing University of Chinese Medicine*, *Nanjing*, *Jiangsu* 210008, *China*

[2] *Department of Plastic and Reconstructive Surgery*, *Shanghai Ninth People's Hospital*, *Shanghai Jiao Tong University School of Medicine*, *Shanghai* 200025, *China*

[3] *Center for Reproductive Medicine and Obstetrics and Gynecology*, *Nanjing Drum Tower Hospital*, *Clinical College of Nanjing Medical University*, *Nanjing*, *Jiangsu* 210008, *China*

[4] *Center for Reproductive Medicine and Obstetrics and Gynecology*, *Nanjing Drum Tower Hospital*, *Affiliated Hospital of Medical School*, *Nanjing University*, *Nanjing*, *Jiangsu* 210008, *China*

[5] *Center for Molecular Reproductive Medicine*, *Nanjing University*, *Nanjing*, *Jiangsu* 210008, *China*

[6] *Center of Reproductive Medicine*, *Changzhou Maternal and Child Health Care Hospital*, *Changzhou*, *Jiangsu* 213003, *China*

[7] *State Key Laboratory of Reproductive Medicine and Offspring Health*, *Center for Reproductive Medicine and Obstetrics and Gynecology*, *Nanjing Drum Tower Hospital Clinical College of Nanjing Medical University*, *Nanjing*, *Jiangsu* 210008, *China*

[8] *Clinical Center for Stem Cell Research*, *Nanjing Drum Tower Hospital*, *Affiliated Hospital of Medical School*, *Nanjing University*, *Nanjing*, *Jiangsu* 210008, *China*

[9] *State Key Laboratory of Analytic Chemistry for Life Science*, *Nanjing University*, *Nanjing*, *Jiangsu* 210023, *China*

ABSTRACT

Ovarian aging is characterized by a progressive decline in oocyte quality and quantity with age. Icariin (ICA), a flavonoid compound derived from *Epimedium* species, has demonstrated potential as an agent for ovarian restoration. In this study, a subcutaneous implantation system using gelatin methacryloyl (GelMA) hydrogel embedded with ICA was developed to restore ovarian function in aged female mice. Mice were assigned to receive subcutaneous implantation of GelMA alone (GelMA group), GelMA containing ICA (GelMA/ICA group), or a sham operation. Ovarian morphology, serum hormone levels, follicle counts across developmental stages, and reproductive outcomes were evaluated. *In vitro* fertilization (IVF) and embryo culture assays were performed to assess oocyte developmental potential, while a 10 day natural mating trial was conducted to determine fertility restoration. RNA sequencing (RNA-seq) and RT-qPCR were performed to elucidate the underlying molecular mechanisms. Results showed that GelMA/ICA treatment significantly increased ovarian index (0.19±0.01 vs. 0.13±0.01, P<0.0001) and follicle numbers at all developmental stages, including primordial (383.33±151.65 vs. 107.14±32.26, P<0.0001), primary (203.33±83.22 vs. 91.43±27.04, P=0.003), and secondary follicles (154.17±52.00 vs. 59.28±20.50, P=0.029) compared to the sham controls. Hormonal analyses revealed a significant reduction in serum follicle-stimulating hormone (FSH, 11.97±3.53 vs. 53.10± 17.89 ng/mL, P=0.0008), accompanied by elevated anti-Müllerian hormone (AMH, 22.97±2.26 vs. 5.54± 1.56 ng/mL, P<0.0001) and estradiol (E_2, 315.30±37.62 vs. 168.5±14.78 pg/mL, P<0.0001). Oocyte yield and developmental potential improved significantly, as reflected by the increased number of superovulated MII oocytes (17.83±5.15 vs. 4.83±4.79, P=0.0002), and higher

Received: 26 March 2025; Accepted: 08 May 2025; Online: 08 May 2025

Foundation items: This work was supported by the National Natural Science Foundation of China (82271671), Nanjing Drum Tower Hospital Academic Innovation Peak Fund (2024-DF-02), Clinical Trials from Nanjing Drum Tower Hospital (2023-LCYJ-MS-05), Nanjing International Science and Technology Cooperation Program (202201027) to L.D. and Research Project of State Key Laboratory of Reproductive Medicine and Offspring Health (SKLRM-2022D2), Changzhou Medical Center of Nanjing Medical University (CMCM202203), and Clinical Trials from Nanjing Drum Tower Hospital (2022-LCYJ-ZD-02) to H.S.

*Corresponding authors, E-mail: haixiang_sun@nju.edu.cn; 151232031@smail.nju.edu.cn; dinglijun@nju.edu.cn

proportions of two-cell (85.90%±6.16% vs. 50.00%± 10.00%, *P*=0.0009), four-cell (81.67%±9.76% vs. 50.00%±10.00%, *P*=0.0061), and blastocyst stage embryos (64.25%±10.55% vs. 23.33%±15.28%, *P*=0.0067). Live birth numbers were significantly increased following GelMA/ICA treatment (6.90±3.21 vs. 1.72±2.05, *P*=0.0001). Transcriptomic analysis revealed up-regulation of genes associated with cytoskeletal organization (*Vil1*, *Tubb3*), lipid storage (*Soat2*, *Plin4*), oocyte maturation (*Oosp2*), and cytokine secretion (*Cxcl12*). Collectively, these findings suggest that GelMA/ICA hydrogels effectively reverse key hallmarks of ovarian aging and restore reproductive function in aged mice, offering a promising platform for fertility preservation and a novel therapeutic for future investigations into ovarian aging.

Keywords: Ovarian aging; Icariin; Subcutaneous implantation; GelMA; Ovarian reserve

INTRODUCTION

Among all organs, the ovary exhibits some of the earliest and most pronounced signs of aging (Gruhn et al., 2019), marked by a progressive decline in oocyte quantity and quality. This process originates before birth, as the ovarian reserve —comprising a finite pool of primordial follicles —is established during fetal development through the proliferation and assembly of germ cells (Lopez et al., 2023). The gradual attrition of this reserve, governed by complex molecular pathways that regulate follicular maintenance and the timing of ovarian aging, defines the reproductive lifespan and culminates in reduced fertility and menopause, typically manifesting in the fourth decade of life (Isola et al., 2024; Wang et al., 2023). The progressive loss of oocyte number is paralleled by a deterioration in oocyte quality, driven in part by oxidative stress and chronic low-grade inflammation. Excessive accumulation of reactive oxygen species (ROS) disrupts redox homeostasis, inducing lipid peroxidation, DNA fragmentation, and mitochondrial dysfunction in granulosa cells and oocytes. These alterations impair steroidogenic output, notably estradiol synthesis, and compromise follicular development, ultimately accelerating follicular atresia and inducing inflammation (Ainehchi et al., 2020; Khaje Roshanaee et al., 2022; Soltani et al., 2023). With a growing trend toward delayed childbearing, the reproductive consequences of ovarian aging in women of advanced maternal age (≥35 years) have become increasingly evident (Crawford & Steiner, 2015). Progressive ovarian aging disrupts the molecular machinery governing meiotic division, resulting in an increased likelihood of chromosomal separation errors in aged oocytes, significantly raising the incidence of aneuploidy in aged women (Li et al., 2021).

Mitochondrial dysfunction, including deficits in ATP production, accumulation of ROS, and mitochondrial DNA (mtDNA) mutations, represents a central driver of ovarian aging, progressively compromising oocyte quality and reducing fertility. Although interventions such as antioxidant supplementation (e.g., CoQ10) and mitochondrial transplantation have demonstrated therapeutic potential, concerns regarding efficacy, biosafety, and heterogeneity remain unresolved (Ju et al., 2024). A range of strategies has been explored to counteract ovarian aging, including stem cell-based approaches, mitochondrial therapy, antioxidant supplementation, and traditional Chinese medicine, but most have either not undergone rigorous clinical validation or have yielded suboptimal outcomes in translational settings (Bittles et al., 2007). The ovarian metabolic microenvironment, particularly the interaction between granulosa cells and oocytes, plays a critical role in coordinating follicular development and meiotic progression. Senescence-associated disruption of this microenvironment, especially through abnormal mevalonate metabolism in senescent granulosa cells, contributes to disordered meiosis in aging oocytes. The mevalonate pathway facilitates oocyte maturation by activating epidermal growth factor (EGF) signaling via protein isoprenylation, a key process in maintaining oocyte quality (Liu et al., 2023).

Epimedium, a medicinal herb widely used in traditional Chinese medicine, contains a diverse array of bioactive components, including flavonoids, alkaloids, polysaccharides, lignans, volatile oils, and essential trace elements. Among these, flavonoids are the most abundant, with icariin (ICA)—an 8-isopentenyl flavonol glycoside—identified as the principal pharmacologically active compound. ICA contains an isoprenyl side chain that enhances its lipophilicity and binding affinity to membrane-associated P-glycoproteins, reducing its clearance from tissues and prolonging its biological activity (Wang et al., 2016; Xue et al., 2016). ICA has been shown to promote granulosa cell proliferation and up-regulate the expression of *Cyp17* and *Cyp19*, which, in turn, stimulate the secretion of estradiol (E_2) and progesterone (Sheng, 2016; Yang et al., 2013). *In vivo*, oral ICA administration has been reported to increase ovarian, uterine, and pituitary weights and prolong the estrous cycle in female rats (Kang et al., 2012). However, the clinical application of ICA remains constrained by low oral bioavailability, primarily due to hepatic first-pass metabolism and rapid systemic clearance (Liu et al., 2022).

Recent advances in tissue engineering and pharmacotherapy have introduced powerful strategies for the treatment of complex clinical conditions. Among these, gelatin methacryloyl (GelMA), a photo-crosslinkable biomaterial polymerized via ultraviolet (UV) light in the presence of Irgacure 2959, has attracted considerable attention for its favorable biocompatibility, mechanical strength, and tunable physicochemical properties, making it an ideal scaffold for cellular and tissue engineering applications (He et al., 2022; Jiang et al., 2023; Van Den Bulcke et al., 2000). Notably, GelMA hydrogel microspheres have demonstrated promising results in reproductive medicine. For instance, biocompatible GelMA hydrogels fabricated via droplet microfluidics have been used to achieve sustained platelet-rich plasma (PRP) delivery, enhancing endometrial repair and fertility recovery in murine models (Butenko et al., 2024; Yuan et al., 2024). Moreover, GelMA hydrogels have proven capable of supporting the cultivation of human endometrial stromal cells and epithelial gland organoids, underscoring their utility in endometrial tissue modeling (Salisbury et al., 2024). In parallel, injectable GelMA microspheres loaded with miR-21-enriched exosomes have demonstrated therapeutic efficacy in premature ovarian insufficiency (POI) models by reducing granulosa cell apoptosis and improving ovarian function (Pramanik et al., 2024; Zhang et al., 2025).

In light of these advancements, this study introduces a novel subcutaneously implantable GelMA-based sustained-release hydrogel system incorporating ICA, a flavonoid

monomer derived from traditional Chinese medicine, as shown in Supplementary Figure S1. Unlike existing systems, the GelMA/ICA hydrogel provides a biomimetic microenvironment that facilitates cellular adhesion, proliferation, and survival—key features for ovarian tissue regeneration. Beyond its structural role, ICA functions as a bioactive agent targeting key pathways implicated in ovarian aging, particularly the mevalonate metabolic axis. This study is the first to report on the application of GelMA/ICA hydrogels as an innovative therapeutic strategy for ovarian aging, offering a transformative approach that addresses the limitations of conventional delivery systems while enabling long-term restoration of ovarian function.

MATERIALS AND METHODS

Animals and ethics statement

All experimental procedures were performed in accordance with the guidelines of the Experimental Animals Management Committee (Jiangsu Province, China) and were approved by the Ethics Review Board for Animal Studies of Nanjing Drum Tower Hospital, Nanjing University Medical School (Approval No. 2023AE01057).

Synthesis of GelMA

Gelatin (20 g) was dissolved in 50 mL of Dulbecco's phosphate-buffered saline (DPBS) at 50°C under continuous magnetic stirring. Methacrylic anhydride (MA, 12 mL, Sigma-Aldrich, USA) was added dropwise to the gelatin solution and stirred for 3 h at 50°C. The pH was adjusted to 7.5–8.5 every 30 min using 1 mol/L NaOH. The reaction mixture was subsequently dialyzed against deionized water at 40°C for 7 days on a dialysis membrane with a molecular-weight cut-off of 12–14 kDa and lyophilized in a vacuum lyophilizer for 4–7 days after freezing in liquid nitrogen. Different masses of GelMA were weighed, dissolved with 0.5% (w/v) photoinitiator lithium phenyl-2,4,6-trimethylbenzoylphosphinate (LAP), and exposed to UV light (405 nm) for 30–90 s, forming GelMA hydrogels.

Characterization of GelMA hydrogels

Morphological and porosity analysis by scanning electron microscopy: GelMA hydrogels at concentrations of 2.5%, 5%, 7.5%, and 10% were frozen in liquid nitrogen, lyophilized in a vacuum lyophilizer, and subsequently examined by scanning electron microscopy (SEM) to evaluate microstructural features. Porosity and pore size were quantified using ImageJ software. For each concentration, three hydrogel samples were analyzed. From each specimen, two SEM images were randomly selected, and four independent measurements were taken per image.

Mechanical characterization by compression testing: The compressive mechanical properties of GelMA hydrogels (2.5%, 5%, 7.5%, and 10%) were measured using a universal mechanical testing system (Tianyuan, TY-8000, China). Cylindrical hydrogel specimens (diameter: 5 mm; height: 5 mm) were subjected to compression at a rate of 0.5 mm/min until reaching 50% strain. Each concentration group included at least three replicates.

Evaluation of *in vitro* release and degradation: To evaluate ICA release kinetics, ICA-loaded composites were dispersed into bottles with phosphate-buffered saline (PBS) and incubated in a thermostatically controlled shaker at 37±1°C with agitation at 80–100 rpm. At predetermined time points (1 h, 3 h, 6 h, 12 h, 24 h, 72 h, 120 h, and 360 h), 1 mL of the solution was collected, with an equal volume of PBS added to maintain the total volume. ICA absorbance was measured using a microplate reader at a wavelength of 405 nm. Each sample was tested in triplicate, and average absorbance values were used to calculate ICA concentrations and cumulative release percentages. Drug release curves were generated by plotting sampling time versus cumulative release percentage.

Hydrogel degradation was assessed by preparing GelMA hydrogels of varying concentrations and recording their initial mass (W_0). Each sample was immersed in 1 mL of PBS within individual microcentrifuge tubes and incubated in a constant-temperature shaker at 37°C and 100 r/min. At predetermined time points, PBS was removed, and the remaining hydrogel was collected and weighed to obtain residual mass (W_t). The hydrogel degradation rate was calculated using the following formula:

$$\text{Degradation rate}(\%) = \frac{(W0 - Wt)}{W0} \times 100\% \quad (1)$$

Assessment of *in vitro* GelMA hydrogel biocompatibility

Cell proliferation assay: The cytocompatibility of GelMA hydrogels was assessed using human foreskin fibroblasts (HFFs) and human ovarian granulosa cells (KGNs) via a direct contact method. The optimal concentration of ICA for mouse granulosa cells was determined to be 50 μg/L using the Cell Counting Kit-8 (CCK-8) assay. To prepare the hydrogel extract, freshly fabricated ICA-loaded hydrogels were incubated in 10% FBS-free medium at 37°C for 24 h. Both cell types were seeded in 96-well plates at a density of 3×10^4 cells/mL and cultured at 37°C with 5% CO_2 for 24 h. After 24 h, cell morphology and attachment were observed under a microscope. The medium was then removed, and 100 μL of appropriate medium (CTL, 50 μg/L of ICA (ICA group), 7.5% (w/v) GelMA hydrogel (GelMA group), and 7.5% (w/v) GelMA hydrogel combined with ICA (GelMA/ICA group)) was added to each well. The plates were incubated for an additional 24 h. Cell proliferation was assessed using CCK-8 solution. After incubation at 37°C for 2 h, optical density (OD) at 450 nm was measured using a microplate reader. Cell viability was quantified based on OD values. Each experiment was conducted in triplicate (n=3).

Live-dead viability assay: To assess cell viability, GelMA hydrogel extracts were prepared by incubating the hydrogels in 10% FBS-free medium at 37°C for 24 h. After incubation, cell culture medium in the 96-well plates was aspirated, followed by the addition of 100 μL of the prepared hydrogel extract. Cells were then incubated at 37°C for 24 h. Following treatment, calcein-AM and propidium iodide (PI) staining solutions were prepared according to the live-dead staining kit instructions. After removing the hydrogel extract, the staining solutions were added to each well, and the plates were incubated at 37°C for 30 min. Each condition was tested in triplicate (n=3). After staining, cells were imaged using a fluorescence microscope, with viable cells fluorescing green (calcein-AM) and non-viable cells fluorescing red (PI).

In vivo animal experiment and evaluation

Based on established lifespan correlations, one human year is approximately equivalent to 9 days in mice (Dutta & Sengupta, 2016). Sixty C57BL/6 female mice aged 9.5 months were randomly divided into three groups: sham group (n=20): aged

mice treated with sham operation; GelMA group (n=20): aged mice treated with subcutaneous implantation of 7.5% GelMA hydrogel; and GelMA/ICA group (n=20): aged mice treated with subcutaneous implantation of 7.5% GelMA hydrogel containing ICA. Mice were weighed prior to the procedure and anesthetized with isoflurane. In a supine position, a small surgical field in the dorsal neck region was prepared and disinfected with 70% alcohol. A longitudinal skin incision (approximately 0.5 cm) was made. In the sham group, the incision was sutured without any treatment. In the GelMA group, GelMA hydrogel was implanted under the skin. In the GelMA/ICA group, GelMA hydrogel containing 2.1 mg of ICA was implanted under the skin. All incisions were sutured, and the surgical area was disinfected again with 70% alcohol. Following recovery from anesthesia, the mice were returned to their cages. Intramuscular penicillin (4.8 mg/mouse) was administered for three consecutive days to prevent post-operative infection. General health parameters including activity, food intake, urine output, and general behavior were monitored throughout the experimental period.

Assessment of ovarian function: Two weeks post-implantation, mice were anesthetized, and blood was collected via orbital extraction. Major organs, including the heart, liver, spleen, lungs, kidneys, and ovaries, were collected and fixed in 4% paraformaldehyde (PFA). The fixed ovaries were sliced into 5 μm sections and stained with hematoxylin and eosin (H&E). Follicles containing visible oocyte nuclei were counted, and the total number of follicles was estimated by multiplying the observed count by five. Follicles were classified based on Stubbs criteria (Myers et al., 2004). H&E staining was also performed on major organ sections (5 μm) to assess histopathological changes.

Serum hormone levels were measured using follicle-stimulating hormone (FSH), anti-Müllerian hormone (AMH), and E_2 enzyme-linked immunosorbent assay (ELISA) kits (E-EL-M0511, E-EL-M3015, E-OSEL-M0008, Elabscience, China). Blood samples were left overnight at 4°C, followed by centrifugation at 3 000 rpm for 10 min to isolate plasma, which was aliquoted and stored at −80°C until analysis. Samples were thawed on ice, and hormone concentrations were determined by ELISA kits according to the manufacturer's instructions. Absorbance (OD) was recorded at 450 nm, with blank wells used for calibration.

***In vitro* fertilization (IVF) and embryo culture:** Sperm were harvested from the epididymides of 8-week-old male C57BL/6 mice and capacitated for 1 h (37°C, 5% CO_2) in HTF medium (Sigma, MR-070-D, USA). Ovulated oocytes were co-incubated with capacitated sperm for 4 h to allow fertilization. The resulting zygotes were cultured in KSOM medium (Sigma, MR-106-D, USA) at 37°C under 5% CO_2.

Fertility experiments: To assess fertility, female mice were mated with proven fertile males at a ratio of 2:1 for 10 days beginning 2 weeks after treatment. The day a vaginal plug was detected was recorded as 0.5 days of pregnancy. Mice were euthanized after 18.5 days of gestation, and the number of embryos was counted following dissection of the uterus.

Hemolysis experiments: Mouse red blood cells were collected to evaluate hemocompatibility. Hydrogel samples were weighed and transferred into microcentrifuge tubes, each containing 1 mL of red blood cell suspension diluted in PBS (pH 7.4). The tubes were incubated at 37°C for 2 h. A 2% erythrocyte PBS suspension and 2% erythrocyte Triton X-100 (1% v/v) suspension served as the blank and positive controls, respectively, while the hydrogel samples constituted the experimental group. After incubation, 100 μL of supernatant was transferred to a 96-well plate, and absorbance at 570 nm was determined using a microplate reader. Each group included four parallel replicates (n=4). The hemolysis rate was calculated using the following formula:

$$\text{Hemolysis rate\%} = \frac{(OD_{Experimentgroup} - OD_{Blankgroup})}{(OD_{Positive} - OD_{Blankgroup})} \times 100\% \quad (2)$$

Evaluation of inflammatory response

To assess the local inflammatory response following GelMA hydrogel implantation, wound tissue samples were collected on days 3, 7, and 14 post-surgery, fixed with PFA, and sectioned for H&E and Masson's trichrome staining.

RNA sequencing (RNA-seq)

RNA-seq was performed on ovaries collected from the control and GelMA/ICA-treated groups 2 weeks post-surgery (n=4 per group). Total RNA was extracted, and sequencing libraries were constructed using the TruSeq Stranded mRNA LT Sample Prep Kit (Illumina, USA). Sequencing was performed on the Illumina platform by Shanghai APTBIO (China). Raw sequencing data quality was assessed using FastQC, and low-quality reads were removed. Clean reads were subsequently aligned to the reference genome, and differentially expressed genes (DEGs) were identified using the DESeq2 package, then subjected to Gene Ontology (GO) and Kyoto Encyclopedia of Genes and Genomes (KEGG) enrichment analyses.

RT-qPCR

Gene-specific primers were combined into an assay pool with nuclease-free water to a concentration of 0.1 μmol/L. The RT-qPCR system was prepared as follows: 5 μL of SYBR-Green Mixture, 0.5 μL of Primer-F (10 μmol/L), 0.5 μL of Primer-R (10 μmol/L), 1 μL of cDNA, and 3 μL of ddH_2O. Relative expression levels were calculated using the $2^{-\Delta\Delta Ct}$ method. Primer sequences are provided in Supplementary Table S1.

Immunohistochemistry (IHC)

Ovarian tissue sections (5 μm) were deparaffinized, rehydrated, and incubated at 4°C with the following primary antibodies: PLAC1L (OOSP2) (1:200, Proteintech, 17343-1-AP), FOSL1 (1:500, ABclonal, A5372, China), and RASAL1 (1:500, ABclonal, A15114, China). A horseradish peroxidase (HRP)-conjugated secondary antibody (rabbit anti-mouse IgG H&L, Proteintech, No. PK10006, China) was applied for detection. Transverse ovarian sections were randomly selected from each group, and antibody expression was evaluated by calculating the percentage of positively stained areas.

Statistical analysis

Histological assessments were performed independently by two observers, and average values were used for analysis. All experiments were repeated at least three times, with data presented as mean±standard deviation (SD). For RNA-seq, DEGs were identified using the DESeq2 package in edgeR, with a significance threshold of |log2 fold change|>1 and adjusted P-value (P-adjust) <0.05. For comparisons involving more than two groups, one-way analysis of variance (ANOVA) followed by Tukey's *post hoc* test was used to assess statistical significance. For comparisons between two groups, unpaired two-tailed Student's t-tests were applied. The choice

of statistical tests was based on experimental design and data distribution, with data normality verified using the Shapiro-Wilk test. Statistical significance was defined as *: $P<0.05$; **: $P<0.01$; ***: $P<0.001$; ****: $P<0.0001$; ns: Not significant. All statistical comparisons were analyzed using GraphPad Prism v.9.0.

RESULTS

Physical characterization of GelMA/ICA hydrogels

To investigate the integration of ICA within the GelMA hydrogel system, a series of physical assessments were conducted to determine the optimal GelMA concentration based on mechanical strength, drug release kinetics, and degradation profile. GelMA hydrogels were prepared at concentrations of 2.5%, 5%, 7.5%, and 10% (w/v), and their internal morphology was analyzed using scanning electron microscopy. Quantitative analysis of pore size revealed average diameters of 79.63±13.15 μm, 11.44±2.10 μm, 9.45±1.73 μm, and 4.11±0.84 μm, respectively. Significant differences were observed between most concentration groups ($P<0.0001$), except between 5% and 7.5% (w/v) (Figure 1A, B).

The mechanical properties of the hydrogels were next assessed by compression testing. The compressive moduli for the 2.5%, 5%, 7.5%, and 10% (w/v) GelMA hydrogels were 2.10±1.46 MPa, 4.64±1.70 MPa, 45.19±21.58 MPa, and 102.10±60.75 MPa, respectively. Statistically significant differences were detected between the 2.5% and 10% (w/v) groups ($P=0.0082$), as well as between the 5% and 10% (w/v) groups ($P=0.0115$) (Figure 1C, D).

In tissue engineering, drug delivery carriers confer key advantages, including sustained release, targeted delivery, and controllability (Dimatteo et al., 2018). To investigate these properties, the sustained-release and degradation profiles of ICA-loaded GelMA hydrogels were examined across different concentrations (Figure 1E). All formulations exhibited an initial gradual release, with the 2.5% and 5% (w/v) hydrogels demonstrating a relatively rapid release within the first 24 h. Among the tested concentrations, 7.5% (w/v) GelMA hydrogels achieved the highest cumulative ICA release. Degradation analysis revealed distinct concentration-dependent differences (Figure 1F). The 2.5% and 5% (w/v) GelMA hydrogels fully degraded by day 11, whereas the 7.5% (w/v) GelMA hydrogels fully degraded by day 13. In contrast, the 10% (w/v) GelMA hydrogels exhibited approximately 62% degradation by day 15. These findings indicate that GelMA concentration governs hydrogel architecture, mechanical strength, sustained release, and degradation dynamics. Notably, 7.5% GelMA demonstrated a sustained ICA release peaking at approximately 1 week, aligning with the intended therapeutic timeframe. Based on the integrated analysis of mechanical and pharmacokinetic properties, the 7.5% (w/v) formulation was deemed the most suitable candidate for further experiments.

In vitro and *in vivo* biocompatibility of GelMA/ICA hydrogels

To determine the optimal ICA concentration for subsequent applications, a CCK-8 assay was performed to assess the effects of different ICA concentrations (10, 25, 50, 75, and 100 μg/L) on cell viability (Figure 2A). Results demonstrated that the 50 μg/L concentration significantly enhanced cell proliferation compared to other doses ($P<0.0001$), whereas higher concentrations (75 and 100 μg/L) failed to yield further improvement and exhibited potential cytotoxicity. Following identification of the optimal ICA dose, the biocompatibility of GelMA and ICA was evaluated at the cellular, tissue, and whole-organism levels. *In vitro* cytocompatibility was assessed using HFFs and KGNs. Cells were treated with ICA, GelMA, and GelMA/ICA formulations, and proliferation was subsequently measured via CCK-8 kit. HFF proliferation was significantly enhanced in the ICA group (1.86±0.12) and GelMA/ICA group (1.92±0.05) compared to the control (1.37±0.03) ($P<0.0001$, Figure 2B). KGN proliferation similarly increased in the ICA (0.93±0.041) and GelMA/ICA (0.97±0.07) relative to the control (0.40±0.025) ($P<0.0001$, Figure 2B).

Cell viability was further assessed by live/dead staining using calcein-AM/PI staining. In HFFs, the GelMA group showed no adverse effects, while both the ICA and GelMA/ICA groups demonstrated a significant increase in cell density and a reduction in dead cells compared to the control. No significant changes in KGN cell density or dead cell numbers were observed with the addition of the GelMA extract alone (Figure 2C).

Biocompatibility was further evaluated by measuring the hemolysis rates of 50 μg/L ICA, 7.5% (w/v) GelMA extract, and 7.5% (w/v) GelMA/ICA extract. Notably, the hemolysis rates were 1.17%±0.12%, 1.08%±0.15%, and 1.2%±0.48%, respectively, all significantly lower than the Triton X-100 positive control ($P<0.0001$, Figure 3A, B).

In vivo histopathological analysis revealed no significant abnormalities in the heart, liver, spleen, lungs, or kidneys across the sham, GelMA, and GelMA/ICA groups (Figure 3C). In conclusion, no signs of systemic toxicity or organ damage were observed, indicating good biosafety.

Histopathological evaluation of explanted tissues at 0, 1, 7, and 14 days post-implantation confirmed favorable degradation and tissue integration. H&E staining revealed a time-dependent reduction in hydrogel volume, with complete absorption by day 14 (Figure 3D). Early inflammatory responses were limited to mild neutrophil and lymphocyte infiltration at day 1, which subsided by days 7–14, with no evidence of chronic inflammation (e.g., giant cells, granulomas, or dense lymphocytic aggregates), consistent with previous reports on the biocompatibility of GelMA (Huang et al., 2024). Masson's trichrome staining showed sparsely distributed, non-oriented collagen fibers (green staining) localized primarily at the hydrogel-tissue interface, with no well-defined fibrous capsule formation. By day 14, after complete hydrogel degradation, residual collagen appeared as focal, patchy deposits integrated with surrounding subcutaneous tissue, with no pathological thickening or fibrosis.

Subcutaneous GelMA/ICA implantation restores ovarian function in aged mice

To evaluate the therapeutic efficacy of subcutaneous GelMA/ICA implantation in reversing age-associated ovarian decline, tissue and serum samples were collected 2 weeks post-surgery. Mice receiving GelMA/ICA treatment exhibited significantly higher ovarian index values (0.19±0.01) compared to the sham group (0.13±0.01) ($P<0.0001$, Figure 4A, B). Histological analysis further revealed marked increases in follicle numbers at the primordial, primary, and secondary stages in the GelMA/ICA group relative to sham

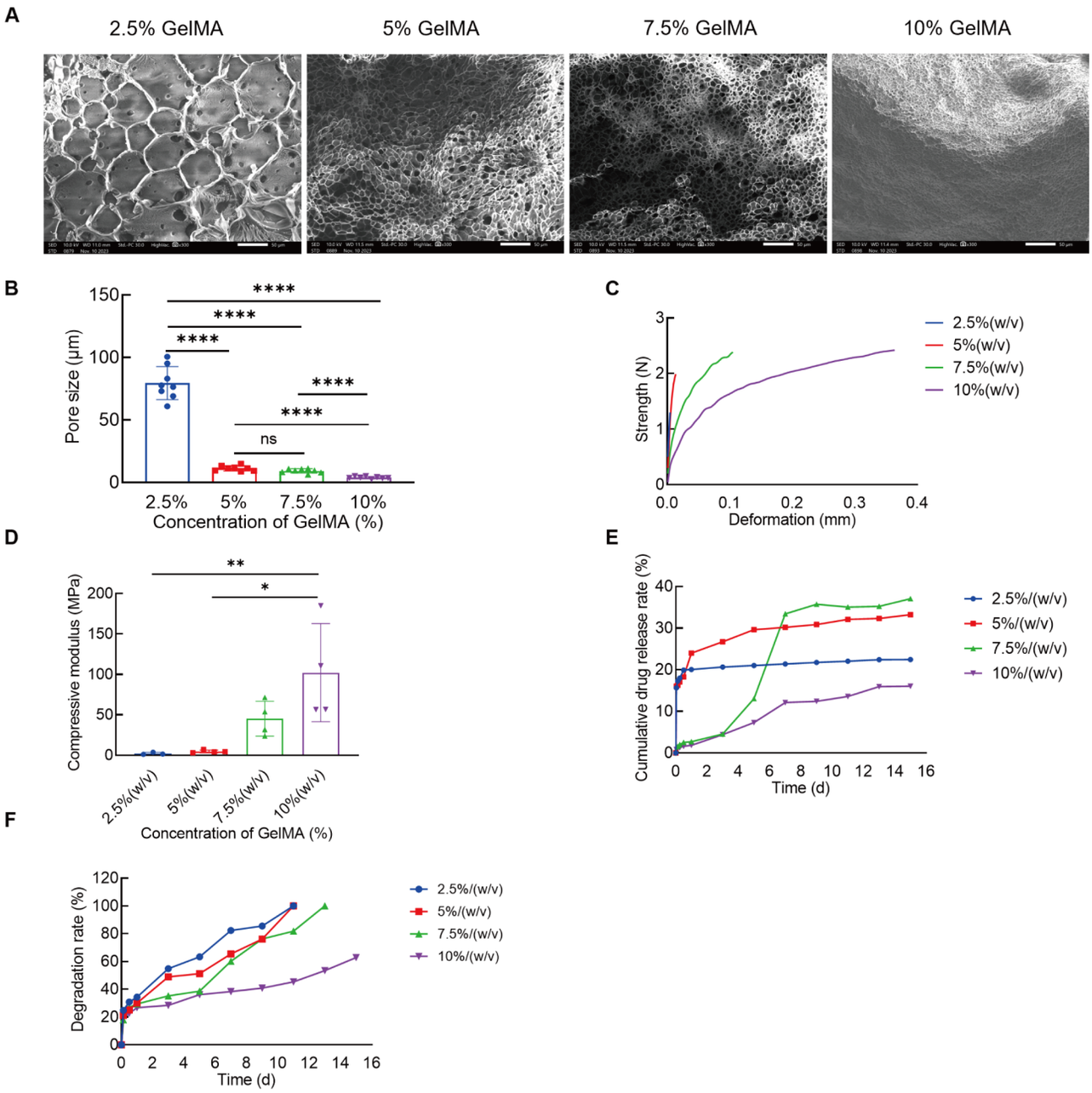

Figure 1 Subcutaneous implantation and physicochemical characterization of GelMA hydrogels

A: Representative microstructures of GelMA hydrogels at 2.5%, 5%, 7.5%, and 10% (w/v) concentrations. Scale bar: 50 μm. B: Quantification of pore size based on SEM imaging for each concentration. Data are mean±SD. C: Force-deformation profiles of GelMA hydrogels across increasing concentrations. D: Compressive modulus measurements of GelMA hydrogels at indicated concentrations. E: Sustained-release curves of ICA in GelMA hydrogels at indicated concentrations. F: *In vitro* degradation profiles of GelMA hydrogels at indicated concentrations over time. Data are mean±SD. ns: Not significant; *: P<0.05; **: P<0.01; ****: P<0.0001.

controls (383.33±151.65 vs. 107.14±32.26, P<0.0001; 203.33±83.22 vs. 91.43±27.04, P=0.003; 154.17±52.00 vs. 59.28±20.50, P=0.029). In contrast, antral follicle counts did not show statistically significant differences among the three groups (GelMA/ICA, GelMA, and sham); however, a non-significant upward trend was observed in the GelMA/ICA group compared to sham controls (54.17±34.70 vs. 27.86±18.45, P=0.052). No significant differences in follicle counts were observed between the GelMA alone and sham groups at any stage (Figure 4C, D).

Endocrine profiling revealed a pronounced reduction in circulating FSH levels in the GelMA/ICA group (11.97±3.53 ng/mL) compared to the sham group (53.10±17.89 ng/mL) (P=0.0008). AMH concentrations were significantly elevated in the GelMA/ICA group (22.97±2.26 ng/mL) compared to the sham group (5.54±1.56 ng/mL), as were E_2 levels (315.30±37.62 pg/mL vs. 168.50±14.78 pg/mL) (P<0.0001) (Figure 4E).

Subcutaneous GelMA/ICA implantation improves embryonic development potential of aged oocytes

To assess the impact of the GelMA/ICA hydrogel on the developmental potential of aged oocytes, *in vitro* IVF experiments were conducted. Mice treated with GelMA/ICA exhibited a significant increase in the number of superovulated MII oocytes compared to the sham group (17.83±5.15 vs.

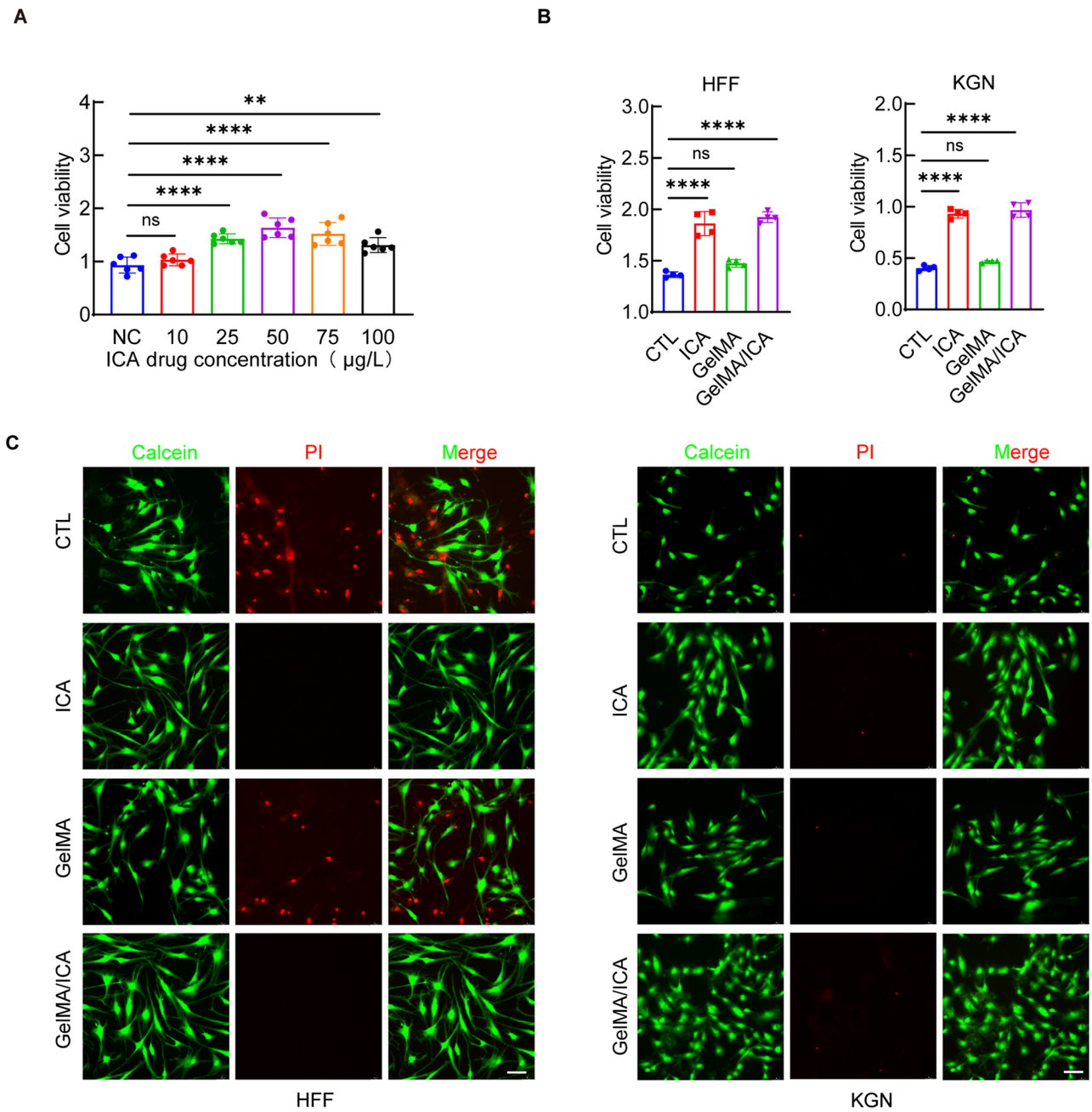

Figure 2 ***In vitro*** **biocompatibility assessment of ICA and GelMA/ICA hydrogels**

A: Proliferation of mouse granulosa cells exposed to different concentrations of ICA. B: Proliferation of human foreskin fibroblasts (HFF) and human ovarian granulosa cells (KGN) under different treatment conditions: Control (CTL), ICA (50 μg/L), GelMA extract (7.5% w/v), and GelMA/ICA extract (7.5% w/v with ICA. Data are mean±SD. C: Live-dead staining of HFFs and KGNs across treatment groups. Scale bar: 50 μm. ns: Not significant; ****: P<0.0001.

4.83±4.79, n=6, P=0.0002) (Figure 5B). Retrieved MII oocytes were fertilized and cultured *in vitro* (Figure 5A, B). The two-cell embryo formation rate was markedly higher in both the GelMA/ICA (85.90%±6.16%, n=107, P=0.0009) and GelMA (88.44%±5.71%, n=42, P=0.0009) groups compared to sham controls (50.00%±10.00%, n=35). Similarly, the four-cell embryo formation rate was significantly elevated in the GelMA/ICA (81.67%±9.76%, n=107, P=0.0061) and GelMA (74.06%±6.43%, n=42, P=0.0322) groups compared to the sham group (50.00%±10.00%, n=35). Blastocyst formation was also enhanced in the GelMA/ICA (64.25%±10.55%, n=107, P=0.0171) and GelMA (59.74%±9.62%, n=42, P=0.0067) groups relative to the sham group (23.33%±15.28%, n=35).

Fertility was further evaluated by mating treated females with fertile male C57BL/6 mice for 10 days, beginning 2 weeks post-surgery. Pregnancy rates were higher in the GelMA/ICA (90%) and GelMA (70%) groups compared to the sham group (45.45%) (Figure 5D). At gestational day 18.5, cesarean section revealed a significantly greater number of live fetuses in the GelMA/ICA group compared to the sham controls (6.90±3.21 vs. 1.73±2.05, n=10, P=0.0001) (Figure 5C, D).

GelMA/ICA up-regulates genes associated with ovarian function

To elucidate the molecular effects of sustained ICA release via subcutaneous GelMA hydrogel implantation on ovarian

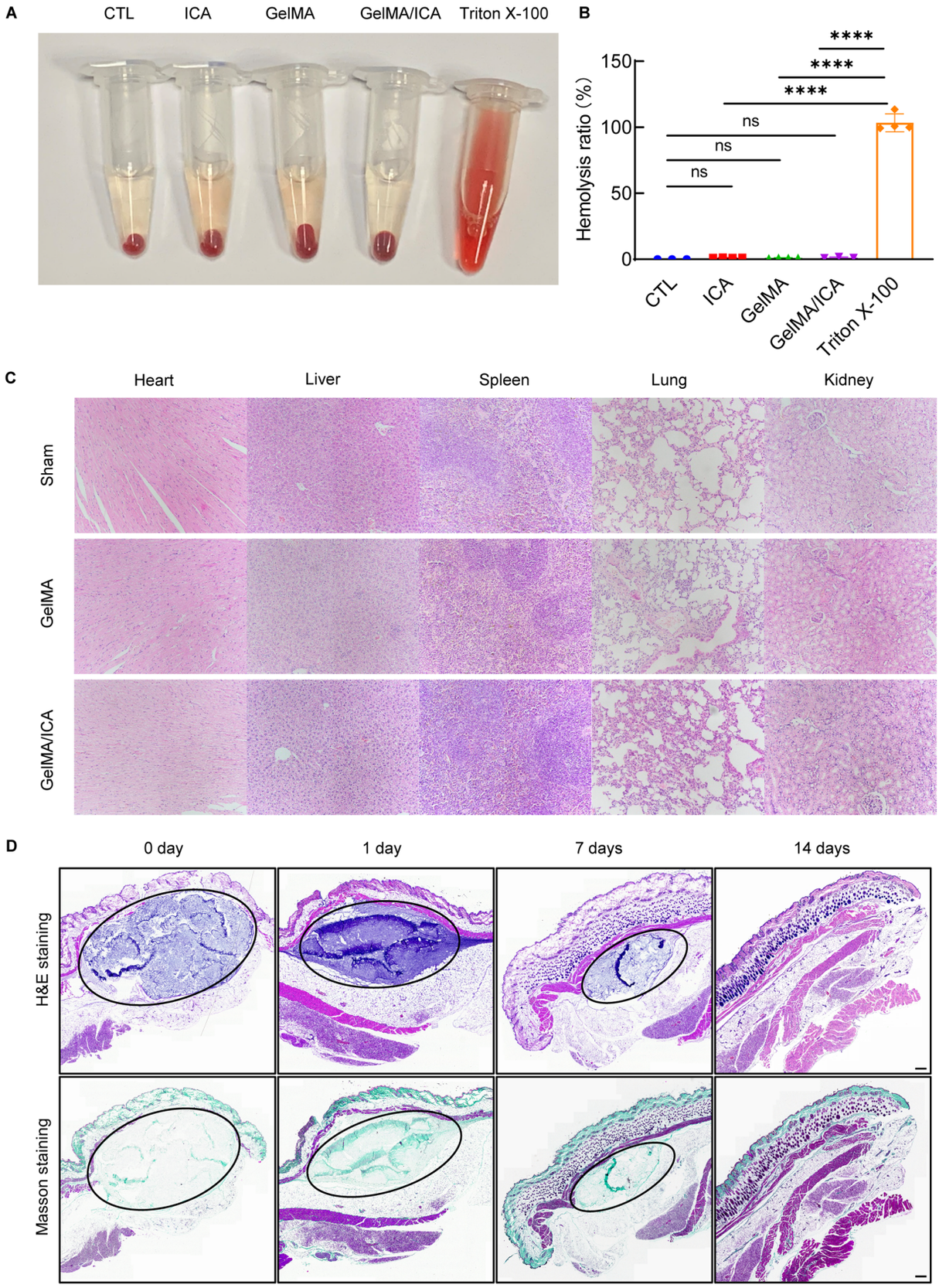

Figure 3 ***In vivo*** **biocompatibility evaluation**

A: Hemolysis assay results for erythrocytes treated with normal saline (CTL), ICA (50 μg/L), GelMA extract (7.5% w/v), GelMA/ICA extract (7.5% w/v with ICA), and 0.5% Triton X-100. B: Quantification of hemolysis rates across treatment groups. Data are mean±SD. C: H&E staining of heart, liver, spleen, lung, and kidney tissues from aged mice in the Sham, GelMA, and GelMA/ICA groups. D: H&E and Masson's trichrome staining of subcutaneous GelMA/ICA hydrogel implants on 0, 1, 7, and 14 days post-implantation; hydrogel boundaries are demarcated by dashed ellipticals. Scale bar: 1 mm. ns: Not significant; ****: P<0.0001.

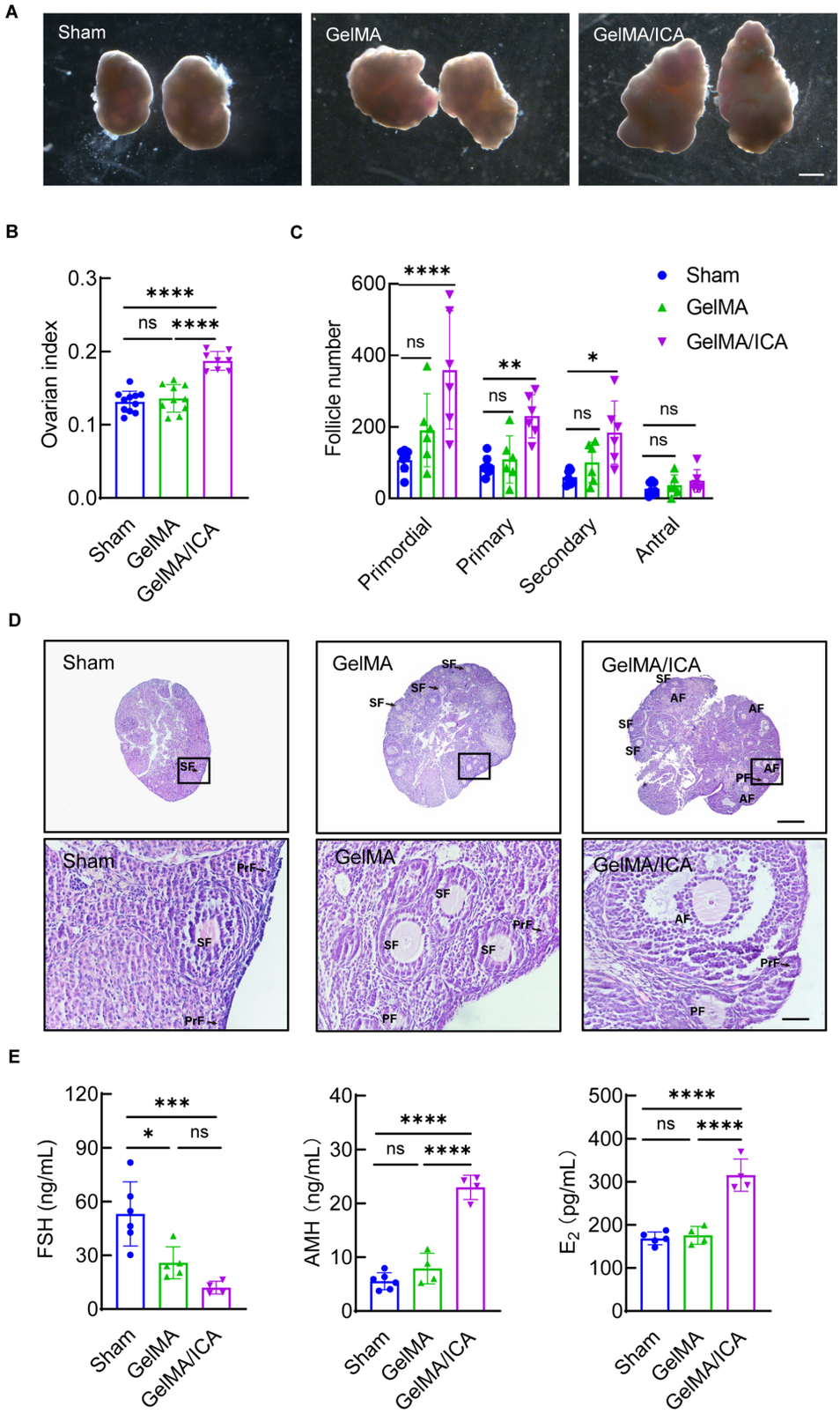

Figure 4 Subcutaneous hydrogel-mediated delivery of ICA enhances ovarian function in aged mice

A: Representative ovarian images from Sham, GelMA, and GelMA/ICA groups. Scale bar: 1 mm. Sham group: aged mice subjected to sham surgery; GelMA group: aged mice subcutaneously implanted with 7.5% GelMA hydrogel; GelMA/ICA group: aged mice subcutaneously implanted with 7.5% GelMA hydrogel containing ICA. B: Ovarian index comparisons among Sham, GelMA, and GelMA/ICA groups. Data are mean±SD. C: Quantification of follicle counts in Sham, GelMA, and GelMA/ICA ovaries. Data are mean±SD. D: H&E-stained ovarian sections in Sham, GelMA, and GelMA/ICA groups. PrF: Primordial follicle; PF: Primary follicle; SF: Secondary follicle; AF: Antral follicle. Scale bar: 20 μm or 200 μm. E: Serum levels of FSH, AMH, and E_2 in Sham, GelMA, and GelMA/ICA groups. Data are mean±SD. ns: Not significant; *: P<0.05; **: P<0.01; ***: P<0.001; ****: P<0.0001.

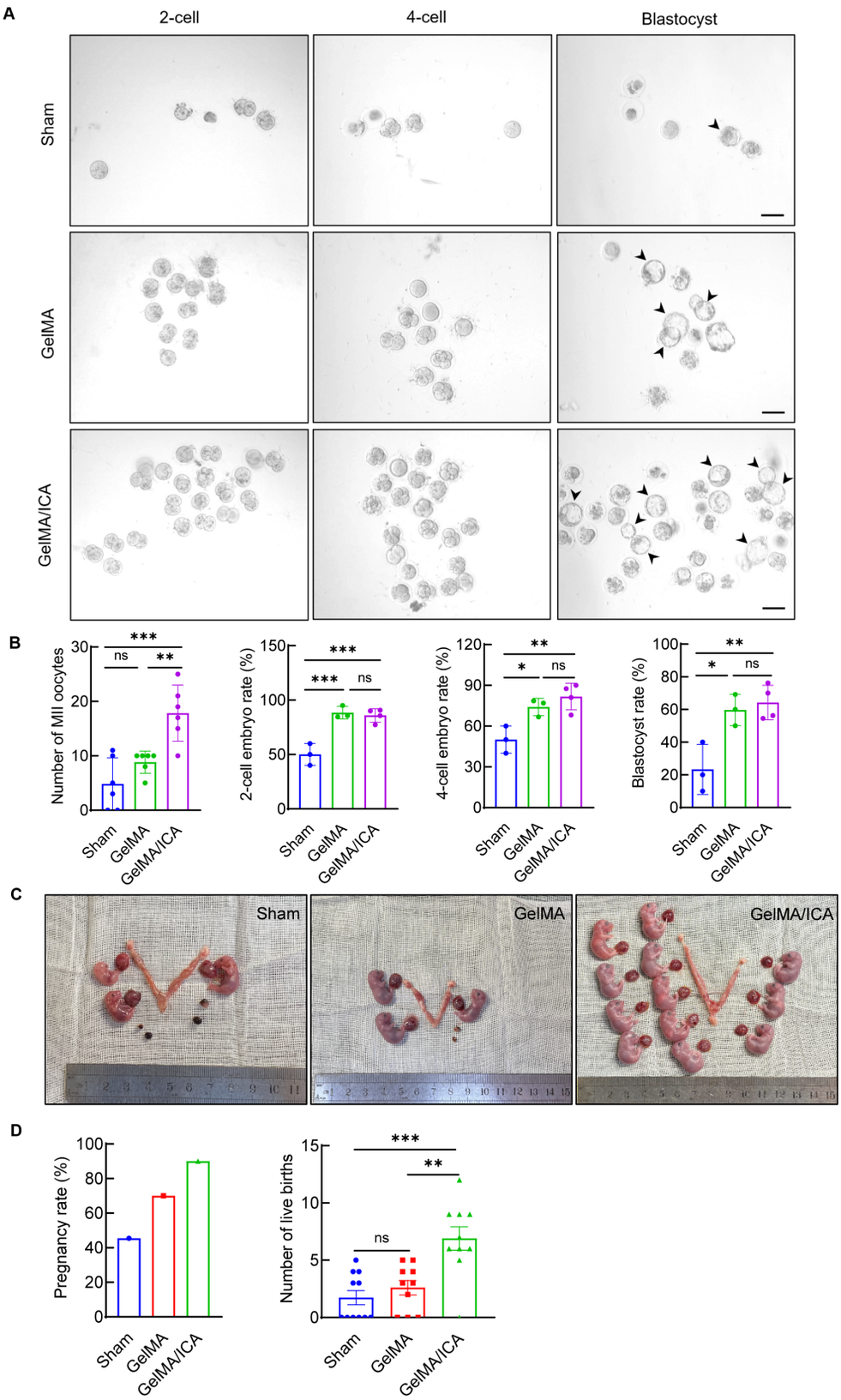

Figure 5 Subcutaneous implantation of the hydrogel sustained-release system enhances embryonic developmental competence and reproductive outcomes in aged mice

A: Representative images of two-cell embryos, four-cell embryos, and blastocysts derived from oocytes of Sham, GelMA, and GelMA/ICA groups. Black arrowheads denote oocytes that progressed to blastulas. Scale bar: 100 μm. Sham group: aged mice subjected to sham surgery. GelMA group: aged mice subcutaneously implanted with 7.5% GelMA hydrogel. GelMA/ICA group: aged mice subcutaneously implanted with 7.5% GelMA hydrogel containing ICA. B: Ratio of oocytes developing into two-cell, four-cell, and blastocyst stages across the three groups. Data are mean±SD. C: Fertility outcomes following mating of treated mice in Sham, GelMA, and GelMA/ICA groups. D: Pregnancy rates and litter sizes in the three groups. Data are mean±SD. ns: Not significant; *: $P<0.05$; **: $P<0.01$; ***: $P<0.001$; ****: $P<0.0001$.

function in aged mice, RNA-seq was conducted on ovarian specimens from eight aged mice (four from the sham group and four from the GelMA/ICA group) (Figure 6A). Differential expression analysis identified 84 significantly up-regulated genes in the GelMA/ICA group compared to the sham group. GO enrichment analysis revealed that these DEGs were primarily enriched in cell communication, signal receptor binding, cell periphery, and plasma membrane (Figure 6B). KEGG pathway analysis further indicated enrichment in cytokine-cytokine receptor interactions and cell adhesion pathways, implicating these processes in the therapeutic mechanism of GelMA/ICA (Supplementary Figure S2).

A heatmap of up-regulated DEGs highlighted key transcripts related to intercellular signaling and structural regulation. Genes involved in cell communication included *Cdkn3*, *Vil1*, *Diras2*, *Dmp1*, *Map3k15*, and *Tubb3*. Signal receptor binding genes included *Oosp2*, *Soat2*, *Cthra1*, *Plin*4, and *Nrcam*. Genes related to cell periphery and plasma membrane functions included *Fosl1*, *Fosb*, *Slc41a3*, *Pde4b*, *Spink4*, *Rasd2*, and *Cxcl12* (Figure 6C). To validate the transcriptomic findings, RT-qPCR was performed on RNA extracted from same ovarian samples. Results confirmed that the mRNA levels of *Tubb3* (P=0.0125), *Vil1* (P=0.0399), *Map3k15* (P=0.0023), *Soat2* (P=0.0014), *Plin4* (P=0.0336), *Oosp2* (P=0.0198), *Rasal1* (P=0.0004), *Rasd2* (P=0.0044), *Fosb* (P=0.0132), *Fosl1* (P=0.0003), and *Cxcl12* (P=0.0135) were significantly increased in the GelMA/ICA group (Figure 6D).

To further corroborate these findings at the protein level, IHC staining was performed for selected key regulators (*Fosl1*, *Oosp2*, and *Rasal1*) known to be involved in ovarian aging. IHC analysis showed strong consistency with both the RNA-seq and RT-qPCR data (Supplementary Figure S3). FOSL1 expression was significantly increased in follicular granulosa cells (18.68%±3.85% vs 5.95%±2.39%, P<0.0001), OOSP2 was significantly up-regulated in oocytes (18.12%±5.13% vs. 7.32%±3.41%, P=0.0016), and RASAL1 showed higher expression in both oocytes and ovarian stromal cells in the GelMA/ICA group (15.64%±5.85% vs. 6.27%±1.90%, P=0.0039).

DISCUSSION

In this study, subcutaneous delivery of the ICA-loaded GelMA hydrogel significantly improved ovarian function and embryonic potential in aged mice. Notable findings included significant elevation of the ovarian index, increased follicular counts across all developmental stages, reduced circulating FSH concentrations, and increased AMH and E_2 levels. These endocrine and morphological improvements were paralleled by enhanced embryogenic potential, as demonstrated by higher rates of progression to the two-cell, four-cell, and blastocyst stages in IVF assays. These findings suggest that the hydrogel system not only increased oocyte yield but also improved intrinsic oocyte quality, thereby promoting embryonic developmental capacity. RNA-seq and RT-qPCR analyses further revealed that this functional recovery was accompanied by the transcriptional activation of genes involved in ovarian function, cytoskeletal dynamics, lipid metabolism, oocyte maturation, and cytokine signaling, collectively implicating a broad reactivation of ovarian regulatory networks (Supplementary Figure S4).

This study also established GelMA hydrogel as a robust drug carrier for sustained-release therapeutics in reproductive tissue engineering. Notably, the hydrogel exhibited favorable biocompatibility, controllable mechanical properties, and enzymatically tunable degradation, making it well suited for incorporation with the bioactive traditional Chinese medicine monomer ICA. Comprehensive *in vitro* and *in vivo* assessments confirmed the absence of cytotoxicity, hemolytic activity, or adverse tissue responses following implantation. Structurally, GelMA assembles into a photo-crosslinked three-dimensional network that supports cell adhesion, proliferation, and migration, while simultaneously serving as a drug carrier for localized, controlled release of bioactive molecules (Chen et al., 2024). GelMA-based formulations have been applied to accelerate healing in infected diabetic wound models (Chen et al., 2024). Furthermore, in the context of ovarian rejuvenation, mechanical optimization enhances implant stability while ECM-mimetic properties enable GelMA-based constructs such as LAMA2-GelMA to support tissue regeneration and endocrine differentiation (Bao et al., 2023; Huang et al., 2022). These advancements underscore the multifunctional potential of GelMA hydrogel as a precision drug delivery system and as a dynamic scaffold for guiding tissue regeneration and functional recovery.

While GelMA hydrogels demonstrate excellent biocompatibility, tunable mechanical properties, and controllable degradation in short-term studies, the long-term biological impact of their degradation products remains an important consideration. The present findings, together with previous reports, suggest that subcutaneous implantation of these hydrogels induces no overt inflammatory response, as evidenced by the absence of ectopic tissue proliferation or immune cell infiltration. The lack of systemic toxicity likely reflects efficient clearance of gelatin-derived peptides following *in vivo* degradation.

Compared to emerging strategies for improving oocyte function, the GelMA/ICA system offers distinct mechanistic and translational advantages. By modulating cross-linking density and degradation kinetics, the system enables drug release to be temporally aligned with key stages of folliculogenesis, thereby optimizing bioavailability during follicular activation. Although mesenchymal stem cell (MSC) therapy exerts immunomodulatory effects via exosome secretion, it remains limited by inter-donor variability, immunogenicity, and tumorigenic potential (Fu et al., 2024). In contrast, the GelMA-based platforms can accommodate co-delivery of MSCs and their secreted factors, sustaining paracrine signaling to overcome the typically low post-transplantation survival rates of MSCs (Lu et al., 2023). Mitochondrial transplantation, while directly targeting oocyte bioenergetics, faces critical technical barriers, including low delivery efficiency and immunogenic risks of heterologous mtDNA integration (Ju et al., 2024).

Mechanistically, the GelMA/ICA system appeared to activate the MAPK signaling pathway by up-regulating gene networks associated with G protein-coupled receptors and Ras family proteins, thereby facilitating cytoskeletal remodeling, lipid metabolism, and oocyte protein biosynthesis in aged ovaries (Guerrero-Netro et al., 2015). Up-regulation of Fos family genes, which encode tyrosine protein kinases that govern transcriptional activation and cell differentiation (Pettit et al., 2022), was observed and may underpin the restoration of cellular proliferation capacity. Notably, OOSP2, known to drive oocyte maturation via translational enhancement of various downstream genes (Hu et al., 2022; Matsuoka et al., 2023), was also significantly elevated. Transcriptomic, RT-

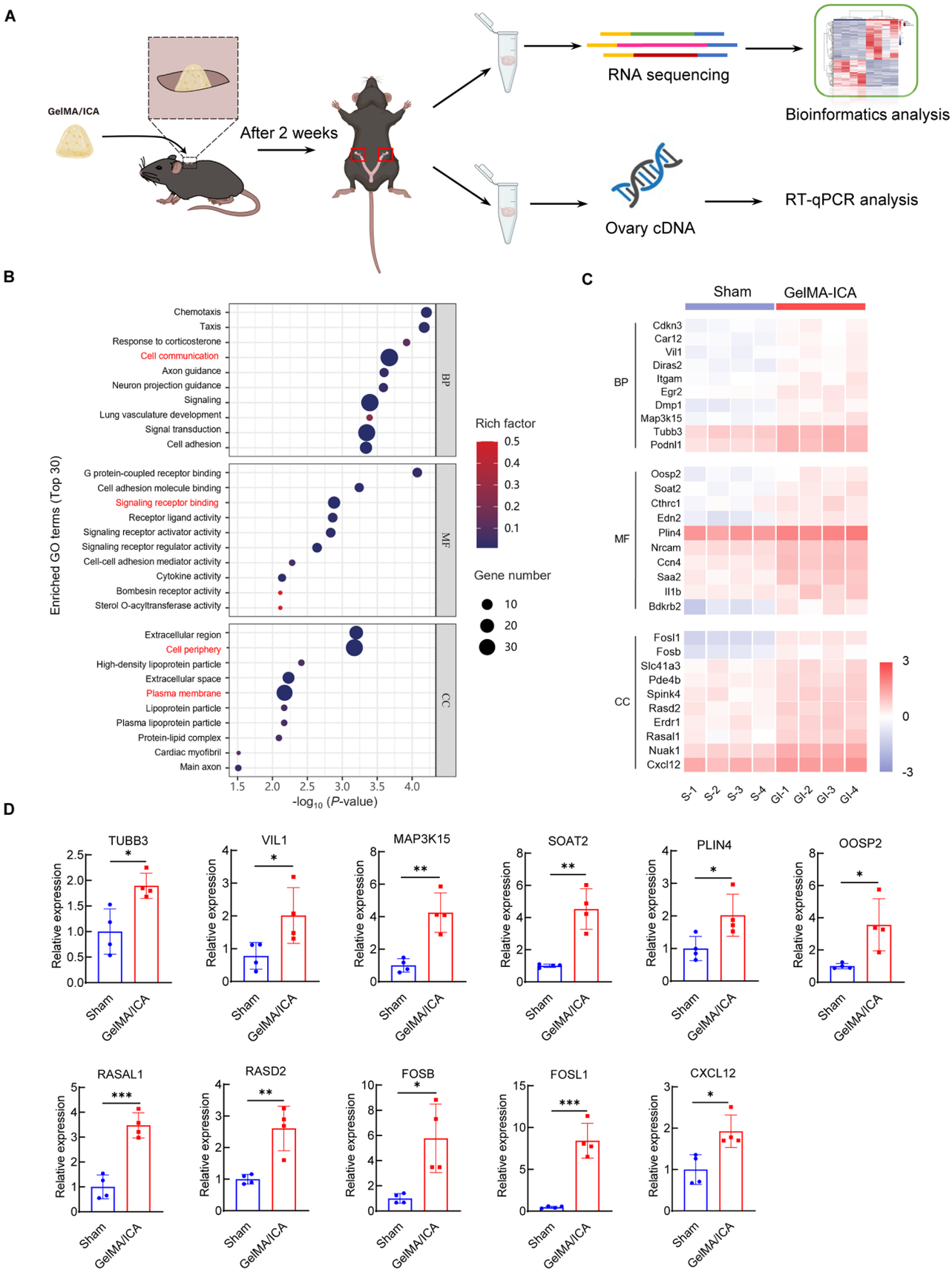

Figure 6 Subcutaneous hydrogel implantation enhances ovarian function in aged mice by up-regulating ovarian-associated gene networks

A: Schematic of RNA-seq analysis workflow. B: GO enrichment analysis highlighting pathways associated with ovarian structure and function. C: Heatmap showing expression profiles of genes enriched in ovary organization and translational regulation. D: Relative mRNA levels of *Tubb3*, *Vil1*, *Map3k15*, *Soat2*, *Plin4*, *Oosp2*, *Rasal1*, *Rasd2*, *Fosb*, *Fosl1*, and *Cxcl12* in Sham and GelMA/ICA groups. *: $P<0.05$; **: $P<0.01$; ***: $P<0.001$.

qPCR, and IHC analyses jointly confirmed the up-regulation of multiple ovarian function-related genes, including the aforementioned ones.

In addition to MAPK signaling, our transcriptomic data suggested that the GelMA/ICA system may enhance mitochondrial function by modulating the mevalonate pathway, potentially through regulation of HMG-CoA reductase activity. This pathway is central to cholesterol biosynthesis and coenzyme Q10 production, both of which are crucial for oocyte maturation and spindle apparatus stability during meiosis. Given the known relevance of mevalonate-derived intermediates to mitochondrial energy homeostasis and cytoskeletal organization, this axis represents a plausible mechanistic target of ICA-mediated ovarian rejuvenation. Nonetheless, direct activation of this pathway remains to be experimentally validated, for instance by assessing transcriptional or post-translational changes in rate-limiting enzymes via RT-qPCR or immunoblotting (Hui et al., 2020; Liu et al., 2023).

Despite the encouraging outcomes, our study has several limitations to consider. First, the short-term evaluation window (2 weeks) precludes assessment of long-term efficacy, particularly regarding sustained ovarian reserve maintenance and offspring health. Second, while murine models provide mechanistic insights, interspecies differences in ovarian aging dynamics necessitate validation in non-human primates. Studies indicate that mice possess a significantly lower follicular reserve than that in humans (approximately 2 000 vs. 1 million) and also exhibit a faster atresia rate. Consequently, translation to clinical contexts will require extension of the GelMA/ICA release profile to match the prolonged human folliculogenesis cycle. Additionally, human ovarian size and stromal density may impede local drug penetration efficiency, necessitating optimization of the hydrogel degradation rate and ICA release kinetics (Sierra-Sánchez et al., 2021). Future investigations should prioritize longitudinal studies tracking ovarian function and multigenerational offspring health, alongside non-human primate trials to establish pharmacokinetic profiles, biodistribution patterns, and safety margins in species with more analogous ovarian physiology.

CONCLUSION

This study demonstrated that subcutaneous delivery of ICA using a hydrogel-based sustained-release platform markedly enhanced ovarian function in reproductively aged mice, as reflected by improved folliculogenesis and restoration of endocrine parameters. Transcriptomic and molecular analyses suggest that the therapeutic effects may be mediated through coordinated up-regulation of genes involved in cytoskeletal organization, lipid metabolism, and oocyte-specific protein synthesis. These findings establish an innovative delivery strategy for targeting ovarian aging and provide a foundation for future translational research into reproductive rejuvenation.

DATA AVAILABILITY

All sequencing datasets were deposited in the Science Data Bank (DOI: 10.57760/sciencedb. j00139.00142), Genome Sequence Archive (GSA, accession No. CRA026053), and National Center for Biotechnology Information database (NCBI, BioProjectID PRJNA1268360).

SUPPLEMENTARY DATA

Supplementary data to this article can be found online.

COMPETING INTERESTS

The authors declare that they have no competing interests.

AUTHORS' CONTRIBUTIONS

L.J.D., H.X.S., G.J.Y., and. Y.F.L.: designed the experiments; J.L.M, L.J.D., X.Y.W, Y.X.W., Z.W.J., L.X.L., N.L., J.D.Z., and Y.Z.: carried out the experiments; J.L.M, L.J.D., C.M.L., H.D.Z., L.C., H.X.S., and G.J.Y.: analyzed the data; J.L.M.: drafted the manuscript; L.J.D. and Y.F.L: revised the manuscript. All authors read and approved the final version of the manuscript.

ACKNOWLEDGMENTS

The authors would like to express our gratitude to Dr. Xin Zhen for invaluable technical assistance in the process of embryo culture.

REFERENCES

Ainehchi N, Khaki A, Ouladsahebmadarek E, et al. 2020. The effect of clomiphene citrate, herbal mixture, and herbal mixture along with clomiphene citrate on clinical and para-clinical parameters in infertile women with polycystic ovary syndrome: a randomized controlled clinical trial. *Archives of Medical Science*, **16**(6): 1304–1318.

Bao BK, Zeng QM, Li K, et al. 2023. Rapid fabrication of physically robust hydrogels. *Nature Materials*, **22**(10): 1253–1260.

Bittles AH, Bower C, Hussain R, et al. 2007. The four ages of Down syndrome. *European Journal of Public Health*, **17**(2): 221–225.

Butenko S, Nagalla RR, Guerrero-Juarez CF, et al. 2024. Hydrogel crosslinking modulates macrophages, fibroblasts, and their communication, during wound healing. *Nature Communications*, **15**(1): 6820.

Chen LP, Wang XY, Ren MJ, et al. 2024. Promoting the healing of infected diabetic wound by nanozyme-containing hydrogel with anti-bacterial inflammation suppressing, ROS-scavenging and oxygen-generating properties. *Journal of Biomedical Materials Research Part B: Applied Biomaterials*, **112**(8): e35458.

Crawford NM, Steiner AZ. 2015. Age-related infertility. *Obstetrics and gynecology clinics of North America*, **42**(1): 15–25.

Dimatteo R, Darling NJ, Segura T. 2018. *In situ* forming injectable hydrogels for drug delivery and wound repair. *Advanced Drug Delivery Reviews*, **127**: 167–184.

Dutta S, Sengupta P. 2016. Men and mice: relating their ages. *Life Sciences*, **152**: 244–248.

Fu Y, Zhang MJ, Sui B, et al. 2024. Mesenchymal stem cell-derived apoptotic vesicles ameliorate impaired ovarian folliculogenesis in polycystic ovary syndrome and ovarian aging by targeting WNT signaling. *Theranostics*, **14**(8): 3385–3403.

Gruhn JR, Zielinska AP, Shukla V, et al. 2019. Chromosome errors in human eggs shape natural fertility over reproductive life span. *Science*, **365**(6460): 1466–1469.

Guerrero-Netro HM, Chorfi Y, Price CA. 2015. Effects of the mycotoxin deoxynivalenol on steroidogenesis and apoptosis in granulosa cells. *Reproduction*, **149**(6): 555–561.

He YZ, Sun M, Wang JR, et al. 2022. Chondroitin sulfate microspheres anchored with drug-loaded liposomes play a dual antioxidant role in the treatment of osteoarthritis. *Acta Biomaterialia*, **151**: 512–527.

Hu WQ, Zeng HT, Shi YN, et al. 2022. Single-cell transcriptome and translatome dual-omics reveals potential mechanisms of human oocyte maturation. *Nature Communications*, **13**(1): 5114.

Huang PY, He YA, Huang CN, et al. 2024. MOF@platelet-rich plasma antimicrobial GelMA dressing: structural characterization, bio-compatibility, and effect on wound healing efficacy. *RSC Advances* 14(41): 30055–30069.

Huang Y, Xu Y, Zhu JC, et al. 2022. An artificial LAMA2-GelMA hydrogel microenvironment for the development of pancreatic endocrine progenitors. *Biomaterials*, **291**: 121882.

Hui S, Cowan AJ, Zeng XF, et al. 2020. Quantitative fluxomics of circulating metabolites. *Cell Metabolism*, **32**(4): 676–688. e4.

Isola JVV, Hense JD, Osório CAP, et al. 2024. Reproductive Ageing: inflammation, immune cells, and cellular senescence in the aging ovary. *Reproduction*, **168**(2): e230499.

Jiang LJ, Huang XY, Tian CC, et al. 2023. Preparation and characterization of porous cellulose acetate nanofiber hydrogels. *Gels*, **9**(6): 484.

Ju WH, Zhao YW, Yu Y, et al. 2024. Mechanisms of mitochondrial dysfunction in ovarian aging and potential interventions. *Frontiers in Endocrinology*, **15**: 1361289.

Kang HK, Lee SB, Kwon H, et al. 2012. Peripubertal administration of icariin and icaritin advances pubertal development in female rats. *Biomolecules & Therapeutics*, **20**(2): 189–195.

Khaje Roshanaee M, Abtahi-Eivary SH, Shokoohi M, et al. 2022. Protective effect of minocycline on *Bax* and *Bcl-2* gene expression, histological damages and oxidative stress induced by ovarian torsion in adult rats. *International Journal of Fertility & Sterility*, **16**(1): 30–35.

Li CJ, Lin LT, Tsai HW, et al. 2021. The molecular regulation in the pathophysiology in ovarian aging. *Aging and Disease*, **12**(3): 934–949.

Liu CM, Zuo W, Yan GJ, et al. 2023. Granulosa cell mevalonate pathway abnormalities contribute to oocyte meiotic defects and aneuploidy. *Nature Aging*, **3**(6): 670–687.

Liu Y, Li T, Sun ML, et al. 2022. ZIF-8 modified multifunctional injectable photopolymerizable GelMA hydrogel for the treatment of periodontitis. *Acta Biomaterialia*, **146**: 37–48.

Lopez J, Hohensee G, Liang J, et al. 2023. The aging ovary and the tales learned since fetal development. *Sexual Development*, **17**(2-3): 156–168.

Lu W, Zeng M, Liu WB, et al. 2023. Human urine-derived stem cell exosomes delivered via injectable GelMA templated hydrogel accelerate bone regeneration. *Materials Today Bio*, **19**: 100569.

Matsuoka K, Bakiri L, Bilban M, et al. 2023. Metabolic rewiring controlled by c-Fos governs cartilage integrity in osteoarthritis. *Annals of the Rheumatic Diseases*, **82**(9): 1227–1239.

Myers M, Britt KL, Wreford NGM, et al. 2004. Methods for quantifying follicular numbers within the mouse ovary. *Reproduction*, **127**(5): 569–580.

Pettit NL, Yap EL, Greenberg ME, et al. 2022. Fos ensembles encode and shape stable spatial maps in the hippocampus. *Nature*, **609**(7926): 327–334.

Pramanik S, Alhomrani M, Alamri AS, et al. 2024. Unveiling the versatility of gelatin methacryloyl hydrogels: a comprehensive journey into biomedical applications. *Biomedical Materials*, **19**(4): 042008.

Salisbury E, Rawlings TM, Efstathiou S, et al. 2024. Photo-cross-linked gelatin methacryloyl hydrogels enable the growth of primary human endometrial stromal cells and epithelial gland organoids. *ACS Applied Materials & Interfaces*, **16**(30): 39140–39152.

Sheng W. 2016. The Effect of Hyperin and Icariin on the Expression of CYP17 and CYP19 in Rat Ovarian Granulosa Cells. Master thesis, Nanjing University of Chinese Medicine, Nanjing. (in Chinese)

Sierra-Sánchez Á, Kim KH, Blasco-Morente G, et al. 2021. Cellular human tissue-engineered skin substitutes investigated for deep and difficult to heal injuries. *npj Regenerative Medicine*, **6**(1): 35.

Soltani M, Moghimian M, Abtahi-Evari SH, et al. 2023. The effects of clove oil on the biochemical and histological parameters, and autophagy markers in polycystic ovary syndrome-model rats. *International Journal of Fertility & Sterility*, **17**(3): 187–194.

Van Den Bulcke AI, Bogdanov B, De Rooze N, et al. 2000. Structural and rheological properties of methacrylamide modified gelatin hydrogels. *Biomacromolecules*, **1**(1): 31–38.

Wang HZ, CHAI YH, Chen YZ, et al. 2016. Research progress on chemical constituents and pharmacological effects of Epimedium. *Asian-Pacific Traditional Medicine*, **12**(7): 63–65. (in Chinese)

Wang XF, Wang LJ, Xiang WP. 2023. Mechanisms of ovarian aging in women: a review. *Journal of Ovarian Research*, **16**(1): 67.

Xue LM, Jiang YP, Han T, et al. 2016. Comparative proteomic and metabolomic analysis reveal the antiosteoporotic molecular mechanism of icariin from *Epimedium brevicornu* maxim. *Journal of Ethnopharmacology*, **192**: 370–381.

Yang LJ, Lu DF, Guo JJ, et al. 2013. Icariin from *Epimedium brevicornum* Maxim promotes the biosynthesis of estrogen by aromatase (CYP19). *Journal of Ethnopharmacology*, **145**(3): 715–721.

Yuan GH, Yu CH, Du X, et al. 2024. Injectable GelMA hydrogel microspheres with sustained release of platelet-rich plasma for the treatment of thin endometrium. *Small*, **20**(47): 2403890.

Zhang XF, Ma LZ, Liu XT, et al. 2025. Sustained release of miR-21 carried by mesenchymal stem cell-derived exosomes from GelMA microspheres inhibits ovarian granulosa cell apoptosis in premature ovarian insufficiency. *Materials Today Bio*, **31**: 101469.